American Mineralogist, Volume 94, pages 1175–1186, 2009

Experimental constraints on rutile saturation during partial melting of metabasalt at the amphibolite to eclogite transition, with applications to TTG genesis

Xiaolin Xiong,[1,2,*] Hans Keppler,[2] Andreas Audétat,[2] Gudmundur Gudfinnsson,[2] Weidong Sun,[1] Maoshuang Song,[1] Wansheng Xiao,[1] and Li Yuan[1,2]

[1]Laboratory of Metallogenic Dynamics, Guangzhou Institute of Geochemistry, CAS, 510640, Guangzhou, China
[2]Bayerisches Geoinstitut, Universität Bayreuth, D-95440 Bayreuth, Germany

Abstract

TiO_2 solubility in rutile-saturated felsic melts and coexisting minerals was determined at 1.5–3.5 GPa, 750–1250 °C, and 5–30 wt% H_2O. TiO_2 solubility in the melt primarily increases with temperature and melt basicity; it increases slightly with water content in the melt, and it decreases with pressure. A general TiO_2 solubility model was obtained and is expressed as: $\ln(TiO_2)_{melt} = \ln(TiO_2)_{rutile} + 1.701 - (9041/T) - 0.173P + 0.348FM + 0.016H_2O$, where TiO_2 and H_2O are in wt%, T is in Kelvin, P in GPa, and FM is the melt composition parameter given by FM = (1/Si)·[Na + K + 2(Ca + Fe + Mn + Mg)]/Al, in which the chemical symbols represent cation fractions. TiO_2 solubility in amphibole, garnet, and clinopyroxene also increases with temperature and empirical equations describing this temperature dependence were derived. These data were used to assess the protolith TiO_2 content required for rutile saturation during partial melting of hydrous metabasalt at the amphibolite to eclogite transition. The results show that only 0.8–1.0 wt% TiO_2 is required for rutile saturation during low-degree (<20%) melting. Rutile is stable up to ~1150 °C with 1.6 wt% TiO_2 in the protolith and 30–40% melting for dehydration melting and up to ~1050 °C and 50–60% melting for fluid-present melting. The data also show that 0.7–0.8 wt% TiO_2 in the protolith is needed for rutile saturation during subsolidus dehydration. Therefore, nearly all basaltic protoliths in deep-crustal settings and subduction zones will be saturated with rutile during subsolidus dehydration and low-degree melting at hydrous conditions.

Archean tonalites-trondhjemites-granites (TTG) are widely accepted to be the products of low-degree melting of metabasalts at the amphibolite to eclogite transition, with rutile being present in the residue. Comparison of natural TTG compositions with our experimental rutile solubility data indicates that the dominant TTG magmas were produced at temperatures of 750–950 °C, which requires that the partial melting occurred at hydrous conditions. Models involving melting at the base of oceanic plateaus are inadequate to explain TTG genesis because the plateau root zones are likely dominated by anhydrous cumulates. A slab-melting model satisfies the requirement of a hydrous metabasalt, which during subduction would melt to produce voluminous TTG melts under high Archean geothermal gradients. The geothermal gradients responsible are estimated to be between 10 and 19 °C/km based on a pressure range of 1.5–2.5 GPa for the amphibolite to eclogite transition.

Keywords: Rutile, amphibolite to eclogite transition, partial melting, TTG, Archean subduction

Introduction

Rutile is a common accessory mineral in high-grade metamorphic rocks, especially in eclogites. It has attracted considerable attention as it may control the budget and distribution of Nb and Ta during metamorphic dehydration and partial melting of subducted oceanic crust and lower continental crust (e.g., Green 1995; Rudnick et al. 2000; Zack et al. 2002; Klemme et al. 2002; Xiong et al. 2005; Xiao et al. 2006; Schmidt et al. 2009). Trace element partitioning experiments have demonstrated that in the presence of rutile, the melt or fluid will be depleted in Nb, Ta, and Ti relative to other elements of similar compatibility (Green and Pearson 1987; Brenan et al. 1995; Stalder et al. 1998; Foley et al. 2000; Klemme et al. 2005; Kessel et al. 2005; Schmidt et al. 2004; Xiong et al. 2005, 2006; Bromiley and Redfern 2008). Archean TTGs have been interpreted as the products of partial melting of metabasalts (amphibolite and/or eclogite) in the subducted oceanic crust or at the base of oceanic plateaus. They have strong Nb-Ta and Ti depletion that is generally attributed to residual rutile (Barth et al. 2002; Xiong et al. 2005, 2006; Bédard 2006). Subduction zone magmas are also characterized by depletion of high field strength elements (HFSE), particularly of Nb and Ta, as compared to both MORB and OIB. This probably reflects the chemical composition of their source region, which was metasomatized by a fluid and, in some cases, perhaps by a melt depleted in these elements (Keppler 1996; Baier et al. 2008).

During subduction or crustal thickening, hydrous basalts undergo successive metamorphic changes with increasing pressure and temperature. Particularly important among these changes is

* E-mail: xiongxl@gig.ac.cn

the amphibolite to eclogite transition, which will lead to dehydration or partial melting of metabasalts due to the breakdown of amphibole and other hydrous phases, finally producing almost dry eclogites. Understanding the role of accessory rutile during these processes requires that rutile stability and rutile/melt as well as rutile/fluid partition coefficients of trace elements are known. During partial melting of metabasalt, TiO_2 is dissolved in the melt and also readily substitutes into residual amphibole, clinopyroxene, and garnet. Saturation in a Ti-rich phase, such as rutile, depends on the TiO_2 content in the protolith as well as on the TiO_2 solubility in the partial melt and coexisting residual phases.

The TiO_2 solubility in silicate melt and minerals varies with composition, pressure, temperature, and perhaps H_2O. Earlier experiments on rutile saturation in silicate melts (Green and Pearson 1986; Ryerson and Watson 1987) show that TiO_2 solubility at high pressures depends mainly on temperature and melt composition, increasing with temperature and melt basicity or melt depolymerization. These experiments demonstrate that TiO_2 solubility in mafic magmas is very high (>5.0 wt% at 1100 °C), which precludes saturation with a Ti-rich phase during mantle melting, whereas felsic melts dissolve little TiO_2, implying possible saturation with a Ti-rich phase in their source region. Recent experiments on rutile saturation in silicate melts (Hayden and Watson 2007; Gaetani et al. 2008) confirm these results and conclusions. The effect of pressure on TiO_2 solubility in silicate melts is relatively small at high pressures (0.8–3.0 GPa) (Green and Pearson 1986; Ryerson and Watson 1987), but the effect is more pronounced at low pressures (Green and Adam 2002), leading to higher TiO_2 solubility at 1 atm and 1350 °C (Gaetani et al. 2008). The influence of H_2O dissolved in the melt has not been explicitly determined by experiments at high pressures, but has been inferred to be small (e.g., Ryerson and Watson 1987; Hayden and Watson 2007). At a low pressure of 0.2 GPa, experiments of Linnen (2005) show that rutile solubility in the subaluminous melt increases with the water content of the melt.

For TiO_2 solubility in minerals, Ernst and Liu (1998) demonstrated that the TiO_2 content in amphibole is strongly dependent on temperature, but nearly independent of pressure. Klemme et al. (2002) conducted experiments on an anhydrous synthetic basalt composition at 3.0 GPa and observed that TiO_2 solubility in clinopyroxene is nearly constant, but in garnet it increases with increasing temperature. Zhang et al. (2003) investigated TiO_2 solubility in coexisting garnet and clinopyroxene at very high pressures (5–15 GPa). They demonstrated that TiO_2 solubility in garnet increases with increasing pressure, which may explain the exsolved rutile microstructures in garnet of natural UHP terranes.

The conditions for rutile saturation during partial melting of dry eclogite at 3.0 GPa and ≥1100 °C have been assessed by Klemme et al. (2002), who demonstrated that rutile saturation is a function of protolith TiO_2 content and temperature. At least ~1.6 wt% TiO_2 is required in the protolith for rutile saturation during partial melting of anhydrous eclogite (see Fig. 2 of Klemme et al. 2002). Using a MORB-like composition with 1.72 wt% TiO_2, Xiong et al. (2005) demonstrated that rutile is stable at pressures generally higher than ~1.5 GPa during partial melting of hydrous metabasalt. However, how much TiO_2 in a protolith is required for rutile saturation at hydrous conditions has not yet been constrained. The TiO_2 content in mid-ocean ridge basalts ranges from 0.7 to 5.0 wt% (Melson et al. 1976). It is not clear whether all natural basalts will be saturated with rutile during dehydration or partial melting at high pressures. In this paper, we present new data on TiO_2 solubility in felsic melt, amphibole, clinopyroxene, and garnet coexisting with rutile at 1.5–3.5 GPa, 750–1250 °C, and ~5–30 wt% H_2O. These data, together with data from the literature on amphibole, clinopyroxene, and garnet are used to assess the protolith TiO_2 content required for rutile saturation during dehydration and partial melting of hydrous basalt under conditions relevant to the amphibolite to eclogite transition. The results are also used to constrain the origin of Archean TTG magmas.

Experimental and analytical methods

Starting materials were five silicate glasses (Tr, Trr, Tr3, Ton, and Ts; see Table 1), with composition ranging from felsic to mafic. The Tr, Trr, Tr3, and Ton glasses are felsic. They were prepared by mixing together analytical grade oxides and carbonates to yield compositions similar to natural trondhjemites and tonalites, except that they have relatively higher TiO_2 contents (2.0–5.0 wt%), which were used to ensure rutile saturation during the experiments. The mixtures were ground under acetone, and after the CO_2 component was removed by sintering, they were fused in Pt crucibles at 1500 °C for 2 h. The quenched glasses were ground again to ensure chemical homogeneity. The Ts starting material, containing 1.72 wt% TiO_2, is a natural basalt glass that was used by Xiong et al. (2005) to investigate the *P-T* conditions for the stability of rutile during partial melting of hydrous basalt. This composition was used here to conduct partial melting experiments to gain more TiO_2 solubility data on melts and minerals (mainly garnet, clinopyroxene, and amphibole) coexisting with rutile. The glasses prepared, together with the melts produced in the partial melting experiments, cover a wide range of melt compositions.

Starting glass (powder) and H_2O were loaded into a $Pt_{95}Rh_5$ capsule that was then welded shut. All experiments were conducted with an end-loaded piston-cylinder apparatus at the Bayerisches Geoinstitut. The assemblage was 12.7 mm in diameter and was composed of outer talc and Pyrex sleeves and a tapered graphite furnace. The sample capsule was placed inside a pyrophyllite sleeve and then inserted into the center of the furnace with Al_2O_3 spacers at both ends. In this assembly configuration, oxygen fugacity should be between the NNO and MW buffers (Xiong et al. 2005). Temperature was measured and controlled with Pt/$Pt_{90}Rh_{10}$ thermocouples (S-type) connected to a Eurotherm controller. Temperatures quoted are believed to be accurate to within ±15 °C due to a gradient over the capsule. Pressure was regulated automatically during the experiments and is accurate to ±0.1 GPa. Experiments were conducted at 1.5–3.5 GPa, 750–1250 °C with ~5–30 wt% H_2O for 48–432 h. The wide ranges of *P*, *T*, H_2O content, and melt composition allow the effects of these variables on TiO_2 solubility to be fully investigated.

Major elements in minerals and quenched melts in the run products were analyzed with a JEOL JXA-8200 electron microprobe at the Bayerisches Geoinstitut.

Table 1. Starting compositions (wt%) used in the experiments

	Tr	Trr	Tr3	Ton	Ts
SiO_2	65.61	68.03	67.46	63.08	48.60
TiO_2	5.00	2.05	2.01	2.03	1.72
Al_2O_3	15.43	15.19	15.40	16.13	16.70
FeO*	2.47	2.58	3.63	6.53	10.53
MnO	0.08	0.07	0.04	–	0.38
MgO	0.97	1.02	0.99	1.92	7.35
CaO	3.09	3.27	3.09	4.52	6.88
Na_2O	4.65	4.75	4.84	3.77	4.18
K_2O	1.82	1.85	1.86	1.03	1.43
P_2O_5	0.10	0.10	0.09	–	0.37
Total	99.18	99.34	99.35	99.62	98.14

Notes: Average of 15–20 spot analyses for the glasses. Tr, Trr, Tr3, and Ton are compositionally similar to natural trondhjemites and tonalites, except that they have higher TiO_2 contents; Ts is a natural basalt glass that was used by Xiong et al. (2005) to investigate the *P-T* conditions for the stability of rutile during partial melting of hydrous basalt. ≤2000 ppm of Nb_2O_5 and Ta_2O_5 was also added to these starting compositions because a parallel study on the Nb, Ta partitioning between rutile and coexisting melt was planned.

Analyses of minerals and quenched melts produced in several runs were also carried out with a JEOL JXA-8800 electron microprobe at the Guangzhou Institute of Geochemistry, CAS. A focused beam was used for mineral analyses and 10–30 μm diameter beams were used for analyses of the quenched melts. The accelerating voltage was 15 kV at a current of 10–30 nA with counting times of 20 s on peak and 10 s for each background for all elements except Na and K, where counting times of 10 s on peak and 5 s for backgrounds were used. TiO_2 analyses of glasses from experiments with $T < 900$ °C were checked using 40–60 s counting times. No discrepancies between results obtained with 20 s and 40–60 s counting time were found, confirming the accuracy of TiO_2 measurement.

Mass balance calculations suggest that there was some volatilization of Na_2O during the glass analyses. The Na_2O contents used to calculate the melt composition parameters (FM) are thus from mass balance calculations. The difference in analytical total from 100% for the quenched melts from runs with >12 wt% H_2O added suggests that there was H_2O loss from these melts due to the drop in pressure during quenching. Here, we assume that the H_2O added into the capsules was presumably dissolved into the melts. This assumption is based on the phase equilibrium experiments of Huang and Wyllie (1986) on tonalite and granite at 1.5 GPa and the phase equilibrium experiments of Bureau and Keppler (1999) on silicate melts + hydrous fluids. The former demonstrated that H_2O saturation solubility in tonalite and granite melts at 1.5 GPa is close to 20 wt%, whereas the latter show that complete miscibility between felsic melts and hydrous fluids will take place at $P \geq 2.0$ GPa and $T > 700$ °C. All our experiments (see Table 2) were conducted at temperatures higher than 700 °C, and the H_2O added into the capsules in the 1.5 GPa runs is lower than 15 wt%. Therefore, the H_2O added into the capsules is believed to have been dissolved into the melts, and aqueous fluid was likely not present during the experiments.

RESULTS

General observation

Thirty-six experiments were performed. Experimental conditions, run products, and compositions of rutile and melt are given in Table 2. Electron microprobe analysis of the quenched melts and the rims of minerals are listed in Tables 3 and 4, respectively. Rutile and melt are present in all the run products. Rutile contains Nb_2O_5, Ta_2O_5, Al_2O_3, and FeO and minor amounts of CaO and MgO in addition to TiO_2. Melt compositions on a water-free basis (Table 2) have SiO_2 contents ranging from 63 to 74 wt%. TiO_2 and other oxides are very homogeneous in the melts, indicating that diffusion in the melt was rapid enough to maintain compositional homogeneity. Crystallization-dissolution equilibrium between rutile and melt was likely achieved, as indicated by nearly identical melt TiO_2 contents in experiments (for example, runs Trr-07 and Trr-12 and runs Trr-05 and Tr-03) with similar run conditions including temperature, pressure, H_2O, and melt composition. Other phases in the products include clinopyroxene, amphibole, garnet, mica, orthopyroxene, quartz, and apatite. Most of these phases were produced only at $T \leq 900$ °C in the runs with trondhjemitic starting compositions (Tr, Trr, and Tr3),

TABLE 2. Experimental conditions, run products, and compositions (wt%) of rutile and melt

Run	*P* (GPa)	*T* (°C)	H_2O added (wt%)	Duration (h)	Phases* (products)	Rutile TiO_2†	Melt SiO_2	Melt TiO_2	Melt FM	Cal-TiO_2
Tr-24	3.5	1050	17.47	70	Rt + melt	90.64(0.49)	71.36(0.91)	0.76(0.03)	1.83	0.73
Tr-15	3.0	1050	14.10	48	Rt + melt	89.07(0.76)	71.10(0.50)	0.74(0.05)	1.83	0.74
Tr-19	1.5	1050	15.16	48	Rt + melt	91.78(0.51)	70.37(0.38)	1.06(0.03)	1.79	0.99
Tr-08	2.0	1150	7.40	48	Rt + melt	89.55(1.07)	70.24(0.13)	1.26(0.04)	1.84	1.29
Tr-07	2.0	1050	8.36	72	Rt + melt	89.72(0.51)	70.87(0.16)	0.78(0.08)	1.83	0.81
Tr-09	2.0	900	9.20	336	Rt + melt + Cpx + Ap	90.38(1.50)	74.01(0.27)	0.25(0.02)	1.46	0.30
Tr-22	2.0	1250	16.35	25	Rt + melt	90.93(0.35)	69.47(0.87)	2.43(0.06)	1.80	2.25
Tr-18	2.0	1150	14.75	48	Rt + melt	91.92(0.25)	69.48(0.54)	1.37(0.05)	1.86	1.49
Tr-04	2.0	1050	13.74	48	Rt + melt	91.21(0.67)	70.76(0.31)	1.01(0.04)	1.85	0.90
Tr-14	2.0	1050	18.76	48	Rt + melt	89.97(0.41)	71.08(0.87)	0.87(0.06)	1.75	0.93
Tr-21	2.0	1050	29.06	72	Rt + melt	90.93(0.41)	70.69(0.39)	1.01(0.04)	1.78	1.11
Tr-02	2.0	900	14.93	168	Rt + melt	91.33(0.76)	71.48(0.28)	0.57(0.04)	1.73	0.37
Tr-03	2.0	850	14.52	146	Rt + melt + Cpx + Ap	89.83(0.78)	72.04(0.77)	0.25(0.02)	1.61	0.24
Tr-01	2.0	800	14.78	145	Rt + melt + Cpx + Mca + Ap	90.14(0.17)	73.44(0.79)	0.19(0.02)	1.52	0.16
Tr-06‡	2.0	900	5.2	168	Rt + melt + Cpx	–	72.80(0.57)	0.26(0.03)	1.52	
Tr3-4	1.5	1050	14.63	75	Rt + melt	93.34(0.40)	70.63(0.60)	1.16(0.03)	1.82	1.01
Tr3-2	1.5	950	13.79	168	Rt + melt	93.95(0.82)	70.93(0.56)	0.56(0.02)	1.74	0.56
Tr3-3	1.5	900	13.59	242	Rt + melt + Cpx	92.65(0.89)	71.52(0.73)	0.34(0.02)	1.58	0.38
Tr3-1	1.5	850	12.96	265	Rt + melt + Am + Ap	90.70(1.45)	71.83 (0.57)	0.27(0.01)	1.74	0.27
Tr3-5‡	1.5	750	10.22	266	Rt + melt + Am + Grt + Mca + Qtz	–	72.74(0.76)	0.11(0.02)	1.40	
Trr-10	2.0	1150	20.15	48	Rt + melt	85.38(0.50)	70.44(0.72)	1.77(0.03)	1.87	1.88
Trr-08	2.0	1050	21.46	96	Rt + melt	83.83(0.98)	70.87(0.99)	0.96(0.03)	1.89	0.95
Trr-11	2.0	950	19.62	168	Rt + melt	82.97(0.71)	71.73(0.42)	0.61(0.03)	1.84	0.51
Trr-07	2.0	900	10.81	270	Rt + melt + Cpx	81.63(0.38)	72.68(0.15)	0.28(0.02)	1.58	0.29
Trr-12	2.0	900	10.56	236	Rt + melt + Cpx	83.50(0.44)	72.61(0.62)	0.29(0.01)	1.61	0.30
Trr-02	2.0	875	19.76	336	Rt + melt + Cpx + Ap	83.21(1.28)	72.58(0.65)	0.22(0.02)	1.58	0.29
Trr-05	2.0	850	20.57	432	Rt + melt + Am + Ap	83.09(1.58)	72.17(0.70)	0.25(0.02)	1.63	0.25
Trr-13	2.0	775	11.73	265	Rt + melt + Cpx + Mca + Qtz + Ap	76.09(15.6)	73.46(0.80)	0.12(0.01)	1.35	0.10
Ton-3	2.0	1050	16.58	72	Rt + melt	91.79(0.55)	67.45(0.51)	1.28(0.04)	2.36	1.13
Ton-5	2.0	1000	14.86	102	Rt + melt	91.67(1.24)	67.36(0.89)	0.73(0.02)	2.37	0.84
Ton-2	2.0	950	9.86	160	Rt + melt + Cpx	93.09(0.60)	68.86(0.94)	0.47(0.02)	1.92	0.51
Ton-1	2.0	900	11.79	280	Rt + melt + Grt + Cpx	92.17(0.61)	71.23(0.80)	0.32(0.02)	1.73	0.35
Ton-4	1.5	1000	11.98	110	Rt + melt + opx	91.90(0.94)	67.42(1.31)	0.87(0.03)	2.34	0.87
Ts-7§	2.0	800	16.32	288	Rt + melt + Cpx + Grt + Am	92.94(2.94)	70.22(1.23)	0.15(0.06)	1.58	0.18
Ts-8§	2.5	925	14.16	192	Rt + melt + Cpx + Grt + Ap	97.31(0.74)	65.86(0.46)	0.46(0.05)	1.95	0.45
Ts-5§	2.5	975	12.13	95	Rt + melt + Cpx + Grt	96.67(0.36)	63.24(1.00)	0.65(0.05)	2.47	0.70

Notes: Average (1σ standard deviation) of 20–50 analysis spots for the rutiles; averages of SiO_2 and TiO_2 for the quenched melts, which are from Table 3 and normalized to 100% on the basis of free-H_2O. FM is the melt composition parameter (see text for the detail). Cal-TiO_2 is the melt TiO_2 solubility calculated by Equation 1 in the text.

* Phase abbreviation: Rt = Rutile; Cpx = clinopyroxene; Am = amphibole; Grt = garnet; Opx = orthopyroxene; Qtz = quartz; Mca = mica; and Ap = Apatite.

† Rutile contains Nb_2O_5, Ta_2O_5, Al_2O_3, and FeO, and minor amounts of CaO and MgO in addition to TiO_2.

‡ Rutile composition in these two runs cannot be obtained due to the very small crystal size (<2 μm).

§ 5.05, 2.93, and 2.43 wt% H_2O were added to the charges of runs Ts-7, Ts-8, and Ts-5, respectively; the H_2O in the melts for these runs was calculated by mass balance in the assumption that the H_2O added into the capsules was dissolved into the partial melts of the basalt starting composition.

TABLE 3. Electron microprobe analysis (wt%) of quenched melts

Run	SiO_2	TiO_2	Al_2O_3	FeO	MnO	MgO	CaO	Na_2O	K_2O	P_2O_5	Total	Na_2O*
Tr-24	64.07(0.91)	0.69(0.03)	14.32(0.38)	0.19(0.2)	0.07(0.02)	0.89(0.05)	3.07(0.09)	3.43(0.24)	1.82(0.07)	0.09(0.02)	88.78(1.26)	4.42
Tr-15	62.81(0.50)	0.65(0.05)	14.31(0.28)	0.30(0.03)	0.07(0.01)	0.93(0.10)	2.99(0.09)	1.69(0.24)	1.72(0.13)	0.08(0.02)	85.53(0.74)	4.39
Tr-19	64.16(0.38)	0.97(0.03)	15.09(0.12)	0.34(0.34)	0.07(0.01)	0.93(0.05)	2.98(0.10)	2.65(0.15)	1.94(0.12)	0.13(0.04)	89.37(0.51)	4.45
Tr-08	64.77(0.13)	1.17(0.04)	15.13(0.11)	0.50(0.03)	0.07(0.01)	0.98(0.02)	3.12(0.04)	2.55(0.08)	1.74(0.02)	0.09(0.02)	90.22(0.20)	4.55
Tr-07	64.29(0.16)	0.71(0.08)	14.83(0.12)	0.40(0.02)	0.07(0.01)	0.97(0.02)	3.08(0.04)	2.15(0.08)	1.73(0.02)	0.10(0.02)	88.42(0.18)	4.45
Tr-09	66.44 (0.27)	0.22(0.02)	14.09(0.20)	0.04(0.02)	0.05(0.01)	0.28(0.02)	2.02(0.03)	1.91(0.50)	1.92(0.32)	0.05(0.02)	87.07(0.88)	4.61
Tr-22	61.59(0.87)	2.16(0.06)	14.37(0.24)	0.03(0.01)	0.06(0.01)	0.92.07()	2.90(0.22)	3.69(0.18)	2.04(0.18)	0.09(0.01)	88.05(1.05)	4.29
Tr-18	63.00(0.54)	1.24(0.05)	15.02(0.13)	0.25(0.02)	0.07(0.01)	0.92(0.02)	2.97(0.07)	2.73(0.15)	2.51(0.32)	0.13(0.03)	88.97(0.80)	4.43
Tr-04	62.47(0.31)	0.90(0.04)	14.32(0.09)	0.32(0.02)	0.07(0.01)	0.96(0.02)	3.06(0.03)	1.45(0.11)	1.64(0.03)	0.09(0.02)	85.38(0.39)	4.35
Tr-14	63.16(0.87)	0.78(0.06)	14.58(0.18)	0.29(0.04)	0.07(0.01)	0.92(0.11)	2.80(0.12)	2.05(0.23)	1.74(0.05)	0.09(0.02)	86.55(0.97)	4.35
Tr-21	62.91(0.39)	0.90(0.04)	14.68(0.15)	0.09(0.01)	0.07(0.01)	0.92(0.02)	2.96(0.05)	2.65(0.07)	1.71(0.04)	0.09(0.01)	87.09(0.60)	4.45
Tr-02	63.98(0.28)	0.51(0.04)	14.77(0.13)	0.12(0.01)	0.07(0.01)	0.88(0.03)	2.97(0.04)	1.32(0.24)	1.68(0.04)	0.10(0.02)	86.41(0.53)	4.42
Tr-03	64.57(0.77)	0.22(0.02)	14.90(0.26)	0.37(0.02)	0.06(0.01)	0.57(0.03)	2.54(0.03)	1.46(0.24)	1.75(0.04)	0.09(0.02)	86.53(1.21)	4.56
Tr-01	65.53 (0.79)	0.17(0.02)	14.30(0.24)	0.46(0.04)	0.05(0.01)	0.34(0.04)	2.26(0.05)	2.14(0.14)	1.50(0.05)	0.06(0.02)	86.82(0.92)	4.54
Tr-06	66.80(0.57)	0.24(0.03)	14.58(0.28)	0.55(0.09)	0.04(0.01)	0.16(0.03)	1.38(0.06)	2.54(0.11)	3.17(0.06)	0.07(0.01)	89.56(0.35)	4.74
Tr3-4	63.91(0.60)	1.16(0.03)	14.69(0.23)	0.27(0.01)	0.04(0.01)	0.90(0.02)	2.99(0.07)	3.07(0.12)	1.78(0.04)	0.08(0.02)	88.78(0.64)	4.57
Tr3-2	63.47(0.63)	0.50(0.02)	15.08(0.17)	0.06(0.01)	0.04(0.01)	0.91(0.03)	3.05 (0.05)	2.46(0.30)	1.77(0.03)	0.08(0.02)	87.28(0.69)	4.46
Tr3-3	64.39(0.73)	0.30(0.02)	15.40(0.22)	0.28(0.02)	0.04(0.01)	0.62(0.02)	2.65(0.05)	2.79(0.33)	1.78(0.03)	0.08(0.02)	88.23(0.75)	4.44
Tr3-1	65.17(0.57)	0.24(0.01)	14.76(0.18)	0.51(0.03)	0.04(0.01)	0.65(0.02)	2.81(0.04)	3.11(0.41)	1.85(0.03)	0.06(0.02)	88.93(0.72)	4.61
Tr3-5	65.96(0.76)	0.10(0.02)	15.41(0.15)	0.46(0.05)	0.02(0.01)	0.17(0.01)	2.14(0.03)	3.64(0.25)	1.73(0.04)	0.01(0.01)	89.58(0.92)	4.64
Trr-10	60.49(0.72)	1.52(0.03)	13.49(0.23)	0.11(0.01)	0.05(0.01)	0.96(0.07)	2.91(0.19)	3.66(0.37)	1.64(0.04)	0.09(0.01)	85.27(0.84)	4.26
Trr-08	62.01(1.09)	0.84(0.03)	13.90(0.21)	0.43(0.10)	0.06(0.01)	0.88(0.21)	2.96(0.55)	3.08(0.23)	1.74(0.09)	0.08(0.02)	86.20(0.96)	4.38
Trr-11	63.40(0.42)	0.54(0.02)	13.94(0.16)	0.07(0.02)	0.05(0.01)	0.93(0.03)	2.96(0.05)	3.94(0.13)	1.75(0.03)	0.09(0.01)	87.89(0.58)	4.44
Trr-07	65.24(0.15)	0.25(0.02)	14.56(0.09)	0.17(0.01)	0.05(0.01)	0.60(0.02)	2.50(0.03)	2.35(0.12)	1.74(0.02)	0.09(0.02)	87.67(0.26)	4.45
Trr-12	65.58(0.62)	0.27(0.01)	14.59(0.63)	0.07(0.01)	0.05(0.01)	0.63(0.02)	2.61(0.04)	2.68(0.20)	1.84(0.03)	0.08(0.02)	88.51(1.20)	4.48
Trr-02	63.82(0.65)	0.20(0.02)	14.36(0.25)	0.23(0.01)	0.05(0.01)	0.53(0.01)	2.40(0.07)	2.10(0.24)	1.70(0.07)	0.07(0.02)	85.53(0.98)	4.40
Trr-05	65.51(0.70)	0.23(0.02)	14.94(0.21)	0.06(0.01)	0.05(0.01)	0.56(0.02)	2.84(0.06)	2.78(0.23)	1.86(0.03)	0.03(0.01)	88.87(0.87)	4.58
Trr-13	64.84(0.80)	0.10(0.01)	14.71(0.34)	0.35(0.02)	0.03(0.01)	0.22(0.01)	1.88(0.05)	4.51(0.16)	1.53(0.03)	0.03(0.01)	88.27(0.88)	4.63
Ton-3	60.32(0.51)	1.14(0.04)	14.91(0.19)	2.15(0.12)	–	1.63(0.10)	4.06(0.41)	2.89(0.22)	1.15(0.05)	–	88.32(0.80)	3.99
Ton-5	61.08(0.89)	0.66(0.02)	14.87(0.40)	2.62(0.33)	–	1.36(0.20)	4.08(0.38)	3.19(0.55)	1.25(0.12)	–	89.18(1.02)	3.89
Ton-2	61.08(0.94)	0.42(0.02)	15.69(0.16)	1.89(0.08)	–	1.02(0.06)	3.31(0.09)	2.36(0.44)	1.14(0.11)	–	87.00(1.03)	4.06
Ton-1	63.05(0.80)	0.28(0.02)	14.94(0.14)	0.93(0.03)	–	0.75(0.03)	3.16(0.06)	1.96(0.19)	1.18(0.04)	–	86.31(0.98)	4.16
Ton-4	61.02(1.31)	0.78(0.03)	15.40(0.18)	2.54(0.10)	–	1.56(0.10)	4.18(0.13)	2.77(0.31)	1.08(0.05)	–	89.41(1.26)	3.87
Ts-7	60.64(1.23)	0.13(0.06)	15.38(0.39)	0.89(0.09)	0.04(0.04)	0.25(0.08)	1.11(0.29)	5.71(0.34)	2.09(0.09)	0.14(0.03)	86.36(1.67)	6.21
Ts-8	57.91(1.15)	0.41(0.05)	16.52(0.47)	0.88(0.13)	0.03(0.03)	0.64(0.01)	1.52(0.11)	5.80(0.78)	3.76(0.38)	0.46(0.03)	87.92(1.46)	6.30
Ts-5	55.05(1.00)	0.56(0.05)	16.10(0.30)	1.99(0.17)	0.07(0.05)	1.16(0.51)	1.72(0.30)	5.63(0.40)	4.35(0.31)	0.38(0.05)	87.05(1.50)	6.13

Note: Average (1σ standard deviation) of 20–30 analysis spots; total iron as FeO.
* Na_2O content calculated by mass balance.

with the exception of clinopyroxene, garnet, and orthopyroxene, which were also present at higher temperatures in the runs with tonalite and basalt starting compositions (Ton and Ts). Orthopyroxene and quartz were observed only in the products of Ton-4 and Tr3-5, respectively. Mica, though not abundant, is observed in three runs, appearing to be muscovite (close to phengite). Amphiboles are Ca rich, with higher Na_2O and K_2O contents in the runs with the basalt starting composition (Ts). Clinopyroxene contains < ~14.0 wt% Al_2O_3, with 8–36 mol% jadeite component and 2.0–6.5 mol% calcium Tschermak's (CaTs) component. Garnet grains are compositionally zoned with cores generally enriched in TiO_2, MgO, and CaO but poor in FeO relative to rims. Temperature has a significant influence on the composition of garnet. In general, almandine content increases with temperature while pyrope content decreases. Although the compositional zoning indicates disequilibrium during garnet growth, one can assume that the rims of the garnet grains approached equilibrium with the melts at the moment of crystallization.

TiO_2 solubility in melts

The TiO_2 solubility in rutile-saturated melts is shown in Figure 1 as a function of melt composition, temperature, pressure, and water content. The results (Figs. 1a, 1b, and 1c) show that TiO_2 solubility in melt markedly increases with increasing temperature and melt basicity as expressed by the FM parameter (Ryerson and Watson 1987), but slightly decreases with increasing pressure, consistent with observations of Green and Pearson (1986) and Ryerson and Watson (1987). In addition, we observed a slight increase in TiO_2 solubility with increasing H_2O content (Fig. 1d). The positive dependence of H_2O content is best illustrated by runs conducted at $P = 2.0$ GPa and $T = 1050$ and 1150 °C. By least-squares analysis for 36 experiments, a general TiO_2 solubility model is obtained as

$$\ln(TiO_2)_{melt} = \ln(TiO_2)_{rutile} + 1.701 - (9041/T) - 0.173P + 0.348FM + 0.016H_2O \quad (1)$$

where TiO_2 and H_2O are in wt%, T is in Kelvin, P in GPa, and FM is the melt composition parameter given by FM = (1/Si)·[Na + K + 2(Ca + Fe + Mn + Mg)]/Al, in which the chemical symbols represent cation fractions. Ryerson and Watson (1987) have discussed the quasi-thermodynamic rationale of the FM parameter. The TiO_2 solubility expression provides a good fit to the data with relative error of <10–15% between experimental and calculated values for all the runs except Tr-02 and Trr-02. The expression deviates somewhat from the model of Ryerson and Watson (1987), because we conducted many experiments with more silicic compositions at lower temperatures compared to their experiments (with $T \geq 1000$ °C), and also because we have considered the effect of H_2O. Calculations show that when H_2O is ignored, relative errors between experimental and calculated TiO_2 values reach 25–40% for experiments at $T < 900$ °C.

TABLE 4. Electron microprobe analysis (wt%) of minerals (except rutile and quartz)

Run	Phase	SiO_2	TiO_2	Al_2O_3	FeO	MnO	MgO	CaO	Na_2O	K_2O	Total
Tr-09	Cpx	51.49(0.95)	1.09(0.47)	13.01(0.87)	6.78(2.55)	0.37(0.06)	7.75(0.49)	14.70(0.21)	3.79(0.42)	0.01(0.01)	99.02(0.21)
Tr-03	cpx	51.68(0.41)	0.82(0.19)	9.53(3.81)	5.56(3.07)	0.44(0.11)	10.64(1.10)	17.72(1.03)	2.84(1.13)	0.00(0.01)	99.25(0.22)
Tr-01	Cpx	52.16(0.19)	0.73(0.23)	13.14(0.59)	4.96(0.11)	0.38(0.06)	8.19(0.28)	15.14(0.52)	4.77(0.08)	0.01(0.01)	99.46(0.18)
	Mca	47.98(0.63)	0.82(0.08)	30.08(0.65)	1.51(0.25)	0.01(0.01)	3.37(0.45)	0.02(0.02)	1.09(0.06)	9.27(0.11)	94.15(0.57)
Tr-06	Cpx	50.42(0.41)	1.04(0.22)	14.40(0.42)	8.22(0.90)	0.34(0.07)	5.96(0.13)	13.02(0.23)	4.83(0.19)	0.07(0.05)	98.31(0.18)
Tr3-3	Cpx	52.38(0.53)	0.88(0.19)	6.46(0.77)	6.97(0.78)	0.24(0.02)	13.81(0.84)	19.94(1.28)	1.39(0.21)	–	100.87(0.79)
Tr3-1	Am	45.82(0.71)	1.32(0.06)	10.65(0.55)	12.56(2.54)	0.19(0.02)	13.97(1.22)	9.43(1.18)	2.26(0.09)	0.38(0.07)	96.57(0.27)
Tr3-5	Am	44.19(0.72)	1.11(0.21)	13.45(1.32)	18.76(1.26)	0.28(0.03)	7.36(0.57)	9.06(0.30)	2.74(1.08)	0.45(0.08)	97.38(0.81)
	Grt	39.00(0.53)	0.73(0.04)	32.69(0.43)	2.22(0.39)	0.17(0.05)	0.33(0.09)	24.08(0.47)	0.05(0.02)	0.01(0.01)	99.46(0.47)
	Mca	49.87(3.04)	0.75(0.05)	35.87(0.95)	1.39(0.19)	0.01(0.01)	1.38(0.06)	0.04(0.02)	1.24(0.69)	6.89(3.25)	97.44(0.57)
Trr-07	Cpx	52.14(0.63)	0.91(0.04)	10.20(0.01)	4.32(0.49)	0.31(0.01)	11.41(0.33)	18.35(0.40)	3.02(0.14)	0.03(0.01)	100.67(0.25)
Trr-12	Cpx	51.62(0.39)	0.97(0.38)	10.60(0.61)	4.56(1.50)	0.29(0.02)	11.63(0.89)	18.36(0.62)	2.81(0.19)	–	100.85(0.96)
Trr-02	Cpx	52.10(1.15)	0.78(0.08)	5.57(2.12)	5.26(1.82)	0.36(0.04)	13.01(1.54)	20.34(1.37)	1.66(0.48)	0.01(0.01)	99.12(0.40)
Trr-05	Am	45.97(0.54)	1.35(0.26)	10.24(0.52)	8.97(0.95)	0.27(0.02)	16.50(0.61)	10.85(0.64)	1.61(0.11)	0.34(0.06)	96.10(0.31)
Trr-13	Cpx	52.18(1.15)	0.75(0.17)	13.95(0.65)	6.59(1.36)	0.34(0.05)	6.49(1.04)	15.51(0.99)	4.55(0.70)	0.02(0.01)	100.39(0.46)
	Mca	50.12(1.71)	0.58(0.05)	33.68(1.28)	1.61(0.15)	0.01(0.01)	1.68(0.08)	0.07(0.06)	2.06(1.07)	8.08(2.13)	97.88(0.31)
Ton-2	Cpx	50.82(0.63)	1.05(0.18)	11.38(0.90)	8.14(2.60)	–	10.24(0.66)	16.14(1.60)	2.65(0.36)	0.01(0.01)	100.73(0.79)
Ton-1	Grt	39.65(0.70)	1.18(0.23)	21.35(0.55)	20.51(2.02)	–	8.52(1.44)	9.18(0.48)	0.07(0.02)	0.01(0.01)	100.56(0.59)
	Cpx	50.73(0.79)	0.81(0.31)	10.69(0.60)	8.99(1.77)	–	10.31(0.76)	16.51(1.15)	2.70(0.19)	0.01(0.01)	100.54(0.70)
Ton-4	Opx	53.76(0.16)	0.23(0.04)	3.47(0.27)	20.08(1.38)	–	22.39(0.88)	1.24(0.16)	0.10(0.04)	0.01(0.01)	101.28(0.24)
Ts-7	Grt	38.33(0.44)	0.82(0.16)	20.63(0.55)	24.76(0.51)	0.96(0.12)	5.40(0.56)	8.86(0.32)	0.19(0.06)	0.01(0.01)	100.14(0.50)
	Cpx	53.01(0.83)	0.75(0.18)	13.13 (0.93)	6.96(0.71)	0.15(0.10)	6.88(0.50)	11.67(0.96)	7.08(0.66)	0.12(0.14)	99.72(0.96)
	Am	42.35(0.87)	1.29(0.18)	14.52(0.92)	12.6391.26)	0.46(0.07)	12.67(1.31)	9.22(0.77)	3.55(0.21)	1.03(0.12)	97.72(0.46)
Ts-8	Grt	39.60(0.30)	0.89(0.20)	21.12(0.42)	18.50(0.43)	0.97(0.38)	10.82(0.88)	8.22(1.09)	0.34(0.22)	0.05(0.03)	100.34(0.54)
	Cpx	52.68 (2.10)	0.96(0.20)	12.39(1.69)	5.59(2.40)	0.13(0.11)	9.31(0.41)	13.09(1.45)	6.42(0.27)	0.02 (0.01)	100.40(0.15)
Ts-5	Grt	38.99(0.23)	1.21(0.25)	20.92(0.26)	14.87(0.31)	1.01(0.17)	14.79(1.02)	8.18(0.78)	0.06(0.01)	0.06(0.03)	99.83(0.87)
	Cpx	52.96(0.86)	0.96(0.23)	12.75(1.32)	6.58(0.93)	0.12(0.11)	7.81(1.87)	12.37(1.13)	6.51(0.68))	0.01(0.01)	99.87(0.76)

Notes: Average (1σ standard deviation) of 7–25 analysis points at rims of the minerals; total iron as FeO. Phase abbreviations as in Table 1.

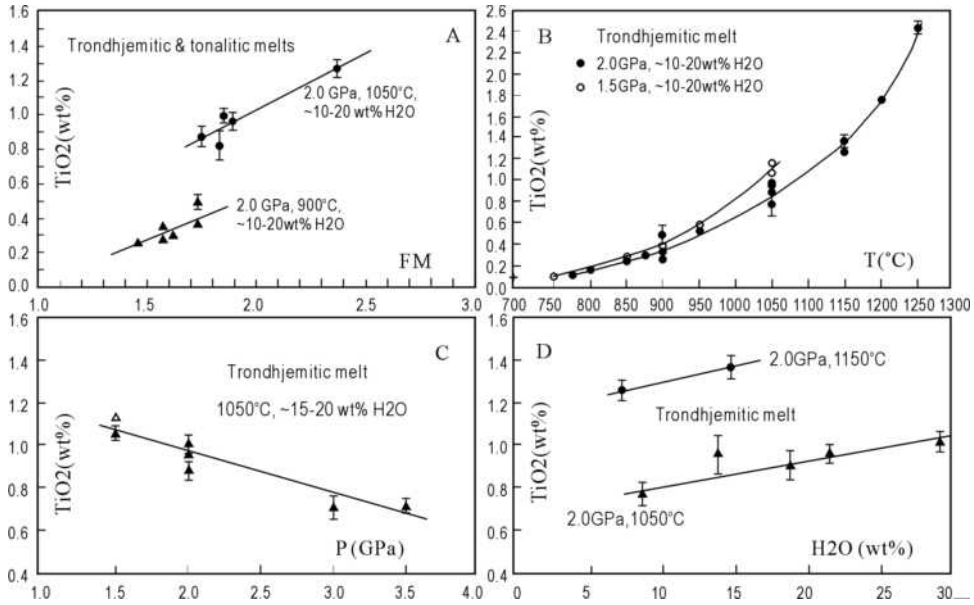

FIGURE 1. TiO_2 solubility in rutile-saturated melts. (**a**) Compositional effect; (**b**) temperature effect (for $T < 900$ °C experiments, the effect is from the combination of temperature and composition due to crystallization); (**c**) pressure effect; (**d**) H_2O effect. Error bars only depicted when larger than symbols.

This is due to the very low TiO_2 solubility in low-temperature silicic melts and thus a small deviation causes a big relative error. Hence, for low-temperature silicic melts, the effect of H_2O cannot be neglected. H_2O may influence the structure of silicic melts and, in turn, changes the activity coefficient and activity (or solubility) of TiO_2 in such melts. This is consistent with predictions of increasing TiO_2 solubility with water content as obtained from spectroscopic studies (Mysen et al. 1982). This is also consistent with the calculated results of Gaetani et al. (2008), who, using their own and published melt TiO_2 solubility data, demonstrated that the addition of H_2O increases the solubility of TiO_2 in silicate melts (see Fig. 5 of Gaetani et al. 2008). Linnen (2005) investigated the effect of water on accessory phase solubility in subaluminous and peralkaline granitic

melts at a lower pressure of 0.2 GPa. He found that solubilities of accessory phases including rutile are affected by the water content of the subaluminous melt (polymerized melt), where the solubilities of all the accessory phases examined increase with the water content of the melt.

TiO_2 solubility in minerals

The TiO_2 solubility (saturation content) in a mineral is a complex function of the composition, structure, and physical conditions of the mineral. Major minerals at the amphibolite to eclogite transition are amphibole, clinopyroxene, and garnet. Titanium readily substitutes into the sixfold-coordinated sites in these minerals (Wood and Blundy 2001). Many phase equilibrium experiments on hydrous basalts at the amphibolite to eclogite transition have been previously reported. Several studies (Sen and Dunn 1994; Rapp and Watson 1995; Ernst and Liu 1998; Forneris and Holloway 2003; Green and Adam 2003; Xiong et al. 2005; Klimm et al. 2008) have clearly described that accessory rutile is present in addition to major minerals ± partial melt in their experimental products. Our results (Table 4) and published data (Appendix Tables 1–3[1]) on TiO_2 solubility in amphibole, garnet, and clinopyroxene at 1.5–2.5 GPa and 650–1150 °C (from subsolidus to suprasolidus) are plotted in Figures 2a, 2b, and 2c, respectively. They include 45 data sets for amphibole, 59 data sets for garnet, and 56 data sets for clinopyroxene. At a given temperature, substantial scatter in TiO_2 solubility is evident from these diagrams, possibly reflecting modest differences in bulk-rock composition and H_2O content used in various experiments and thus differences in the degree of melting and the compositions of minerals and melts. Furthermore, incomplete equilibration may also contribute to the scatter. Nevertheless, TiO_2 solubility in amphibole, garnet, and clinopyroxene clearly increases with temperature (and degree of melting) within the small pressure range considered (1.5–2.5 GPa). It can be seen from Figures 2a, 2b, and 2c that (1) the TiO_2 solubility in amphibole is generally higher than in garnet and clinopyroxene, especially in the case of high temperatures, and (2) with temperature increasing from 650 to 1000–1100 °C, the TiO_2 solubility in amphibole, garnet, and clinopyroxene increases from < ~0.7–0.8 to ~3.5, ~1.8, and ~1.5 wt%, respectively. Using average values of TiO_2, we can parameterize the variation of TiO_2 solubility with temperature in amphibole, garnet, and clinopyroxene as: $\ln(TiO_2) = 4.21–4241/T$ (Fig. 2a), $\ln(TiO_2) = 1.85–2041/T$ (Fig. 2b), and $\ln(TiO_2) = 1.53–1972/T$ (Fig. 2c), where T is in Kelvin, and TiO_2 in wt%.

In addition to the major minerals, minor amounts of hydrous minerals such as zoisite, phengite, lawsonite, chloritoid, and staurolite may occur at relative low temperatures (<800 °C) at the amphibolite to eclogite transition. Available experimental data (Fig. 3 with data listed in Table 4 and Appendix Table 4[1]) show that TiO_2 solubility in these minerals coexisting with rutile-saturated melts or fluids at 1.5–3.0 GPa is generally lower than ~0.8 wt%.

RUTILE SATURATION

Rutile saturation during partial melting

Available experimental data on phase relationships at the amphibolite to eclogite transition in hydrous basalt systems are shown in Figure 4 (data sources below the figure). In the suprasolidus field, amphibolite transforms to eclogite with increasing pressure and temperature, via breakdown of amphibole and plagioclase and crystallization of garnet and clinopyroxene, accompanied by partial melting and melt production. As shown in Figure 4, the solidus is strongly dependent on the H_2O con-

[1] Deposit item AM-09-039, Appendix Tables 1–4. Deposit items are available two ways: For a paper copy contact the Business Office of the Mineralogical Society of America (see inside front cover of recent issue) for price information. For an electronic copy visit the MSA web site at http://www.minsocam.org, go to the American Mineralogist Contents, find the table of contents for the specific volume/issue wanted, and then click on the deposit link there.

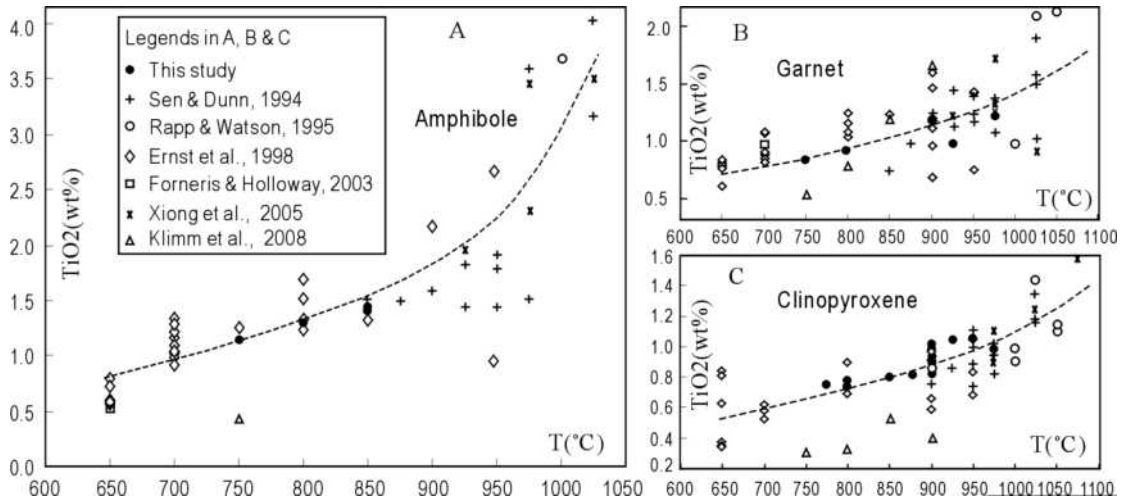

FIGURE 2. TiO_2 solubility in amphibole, garnet, and clinopyroxene coexisting with rutile (650 °C) or rutile-saturated melts (>650 °C) at 1.5–2.5 GPa, showing that the TiO_2 solubility in these minerals increases with increasing temperature. For sources of published data, see Appendix Tables 1–3[1].

tent in the system. The fluid-present or wet solidus is located between 680–750 °C at 1.5–2.5 GPa, whereas the fluid-absent (dehydration melting) solidus is located between ~800 and 900 °C, depending on bulk-rock composition and pressure. The boundaries of amphibole-out for the fluid-absent melting overlap those for fluid-present melting, indicating that the amphibole-out boundary may be controlled mainly by bulk-rock composition. At a given *P-T* condition, melt composition and modes of melt and residual minerals for the fluid-present melting must be different from those for the fluid-absent melting. Melting experiments on metabasalts have shown that at a given temperature and pressure, the melt fraction for fluid-present melting (e.g., Xiong et al. 2005) is markedly larger than that for fluid-absent melting (e.g., Sen and Dunn 1994; Rapp and Watson 1995), and the melt composition for the former is less silicic.

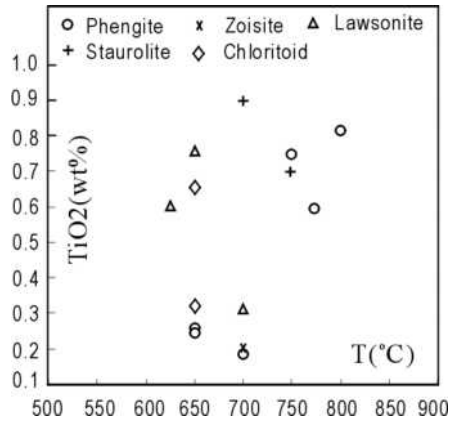

FIGURE 3. TiO_2 solubility in zoisite, phengite, chloritoid, staurolite, and lawsonite coexisting with rutile or rutile-saturated melts at 1.5–3.0 GPa in the basalt–H_2O systems. For sources of published data, see Appendix Table 4[1].

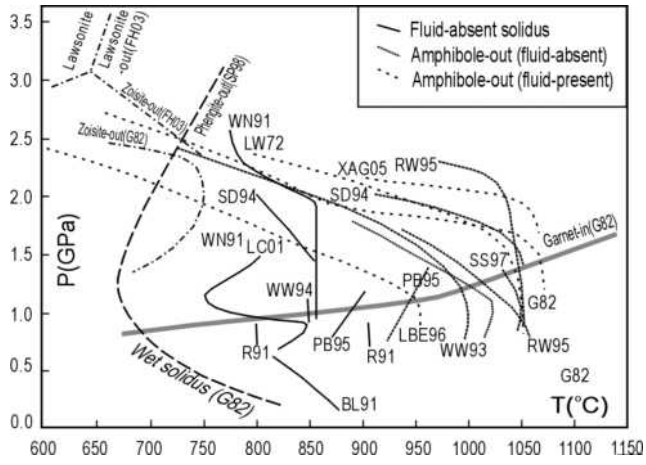

FIGURE 4. Phase relationships for the amphibolite to eclogite transition in the hydrous basalt systems (fluid-absent: H_2O bounded in hydrous minerals; fluid-present: H_2O present in addition to hydrous minerals). See text for details. Data sources: BL91 = Beard and Lofgren (1991); FH03 = Forneris and Holloway (2003); G82 = Green (1982); LC01 = Lopez and Castro (2001); LBE96 = Liu et al. (1996); LW72 = Lambert and Wyllie (1972); PB95 = Patino-Douce and Beard (1995); R91 = Rushmer (1991); RW95 = Rapp and Watson (1995); SD94 = Sen and Dunn (1994); SS97 = Springer and Seck (1997); MN91 = Winther and Newton (1991); WW94 = Wolf and Wyllie (1994); XAG05 = Xiong et al. (2005); SP98 = Schmidt and Poli (1998).

As demonstrated above, the TiO_2 solubility in melt, amphibole, garnet, and clinopyroxene increases mainly with increasing temperature and melt basicity (or melting degree). Therefore, for a protolith with TiO_2 content higher than the required minimum value for rutile saturation, a low degree of melting favors stability of rutile, whereas a higher degree of melting may lead to dissolution and disappearance of rutile. In the case of rutile saturation, the TiO_2 contents in melt and minerals are buffered by rutile. If rutile saturation is not reached (low protolith TiO_2 content and/or high degree of melting), the TiO_2 content in the melt and minerals is controlled by Ti partitioning among minerals and partial melt.

The mass balance of TiO_2 during partial melting of a Ti-bearing protolith can be expressed as TiO_2 (protolith) = TiO_2 (melt) + TiO_2 (residue), where residue = garnet + clinopyroxene ± amphibole ± rutile. For a protolith with a given TiO_2 content, it is easy to estimate whether or not rutile will be saturated during partial melting using the TiO_2 solubility data of melt and minerals presented here and reasonable modes of melt and minerals. When TiO_2 is below saturation (no rutile in the residue), TiO_2 (melt) and TiO_2 (residue) at a given temperature or melt fraction can be calculated iteratively with Ti partition coefficients ($D_{Ti}^{mineral/melt}$) and modes of melt and minerals. $D_{Ti}^{mineral/melt}$ and modes of residual minerals vary with temperature or melt fraction (melting degree). We have used the TiO_2 solubility data for melts and minerals (amphibole, garnet, and clinopyroxene) to obtain $D_{Ti}^{mineral/melt}$ (variations of TiO_2 solubility in melts and minerals with melt composition and temperature are considered). For modes of residual minerals and partial melt used in the calculations, fluid-present melting data are taken from this study (Ts starting material) and Xiong et al. (2005), whereas the fluid-absent melting data are taken from Sen and Dunn (1994) and Rapp and Watson (1995).

For six protoliths, each with TiO_2 at 0.6, 0.8, 1.0, 1.2, 1.4, and 1.6 wt%, respectively, the behavior of TiO_2 during partial melting at the amphibolite to eclogite transition was calculated for four cases: (1) fluid-present melting at 2.5 GPa with eclogite as the residue; (2) fluid-present melting at 1.5 GPa with amphibole-eclogite (<1050 °C) or eclogite (>1050 °C) as the residue; (3) fluid-absent melting at 2.5 GPa with eclogite as the residue; and (4) fluid-absent melting at 1.5 GPa with amphibole-eclogite (<1050 °C) or eclogite (>1050 °C) as the residue. The results are delineated in Figure 5, in which rutile saturation and melt TiO_2 content are expressed as a function of temperature or melt fraction at a given protolith TiO_2 content. Two points are important for understanding the stability of rutile: (1) due to the higher TiO_2 solubility in amphibole as compared to garnet and clinopyroxene, the minimum protolith TiO_2 contents required for rutile saturation in amphibole-eclogite residues at 1.5 GPa (Figs. 5b and 5d) are always 0.1–0.2 wt% higher than those required for rutile saturation in eclogite residues at 2.5 GPa (Figs. 5a and 5c), irrespective of whether the melting is fluid-present or fluid-absent. For all cases, only 0.8–1.0 wt% TiO_2 in the protolith (corresponding to thick dotted curves in Fig. 5) is required for rutile saturation at

low temperature (<900–950 °C) and low degree (<15–20 wt%) of melting; and (2) for a protolith with a given TiO_2 content, the highest temperature of rutile stability (or the temperature of rutile disappearance) for fluid-absent melting is, in general, ~100 °C higher than that for fluid-present melting, irrespective of whether the pressure is 1.5 or 2.5 GPa. For example, for the protolith with 1.6 wt% TiO_2, rutile is stable up to ~1150 °C and 30–40% melting in the absence of fluid (Figs. 5c and 5d) and up to ~1050 °C and 50–60% melting in the presence of fluid (Figs. 5a and 5b).

It should be noted that there is substantial scatter in TiO_2 solubility data of minerals as shown in Figure 2 and the calculated results are only approximate. However, the 0.8–1.0 wt% minimum protolith TiO_2 contents required for rutile saturation at low temperatures (<900–950 °C) is unlikely to be an underestimation. Experiments of Sen and Dunn (1994) show that rutile is stable up to $T > 1000$ °C at 1.5 and 2.0 GPa during the partial melting of a basaltic amphibolite with 1.22 wt% TiO_2, with the produced melts varying from granitic compositions at temperatures close to the solidus to tonalitic compositions at $T > 1000$ °C.

It should also be noted that at the amphibolite to eclogite transition, rutile may not be the only Ti-rich accessory phase. Sphene, ilmenite, and Ti-magnetite may also occur. Rutile is stable at pressures higher than ~1.5 GPa (Xiong et al. 2005), whereas other Ti-rich phases occur generally at lower pressures during the partial melting of metabasalt (Hellman and Green 1979; Ernst et al. 1998). Green and Pearson (1986) have shown that the TiO_2 solubility in a melt in equilibrium with a Ti-rich phase is similar, irrespective of whether the Ti-rich phase is rutile or another phase(s). Thus, the experimental solubility data and calculated results in this paper are believed to be approximately applicable to any case of Ti-saturation. Titanium diffusion is very fast in hydrous melts (Hayden and Watson 2007) and crystallization-dissolution equilibrium of rutile is readily achieved, as indicated by our experiments. Ti-rich accessory phases are always denser than the coexisting melt, and the viscosity of a hydrous melt is quite low. Therefore, Ti-rich phases should separate very quickly from the hydrous melt and are likely to remain in the residue during/after partial melting.

Rutile saturation during subsolidus dehydration

During subsolidus dehydration, the presence of rutile depends on the protolith TiO_2 content and the TiO_2 solubility in fluid and minerals. Early experimental studies (Ayers and Watson 1993) appeared to suggest that rutile is quite soluble in aqueous fluid at

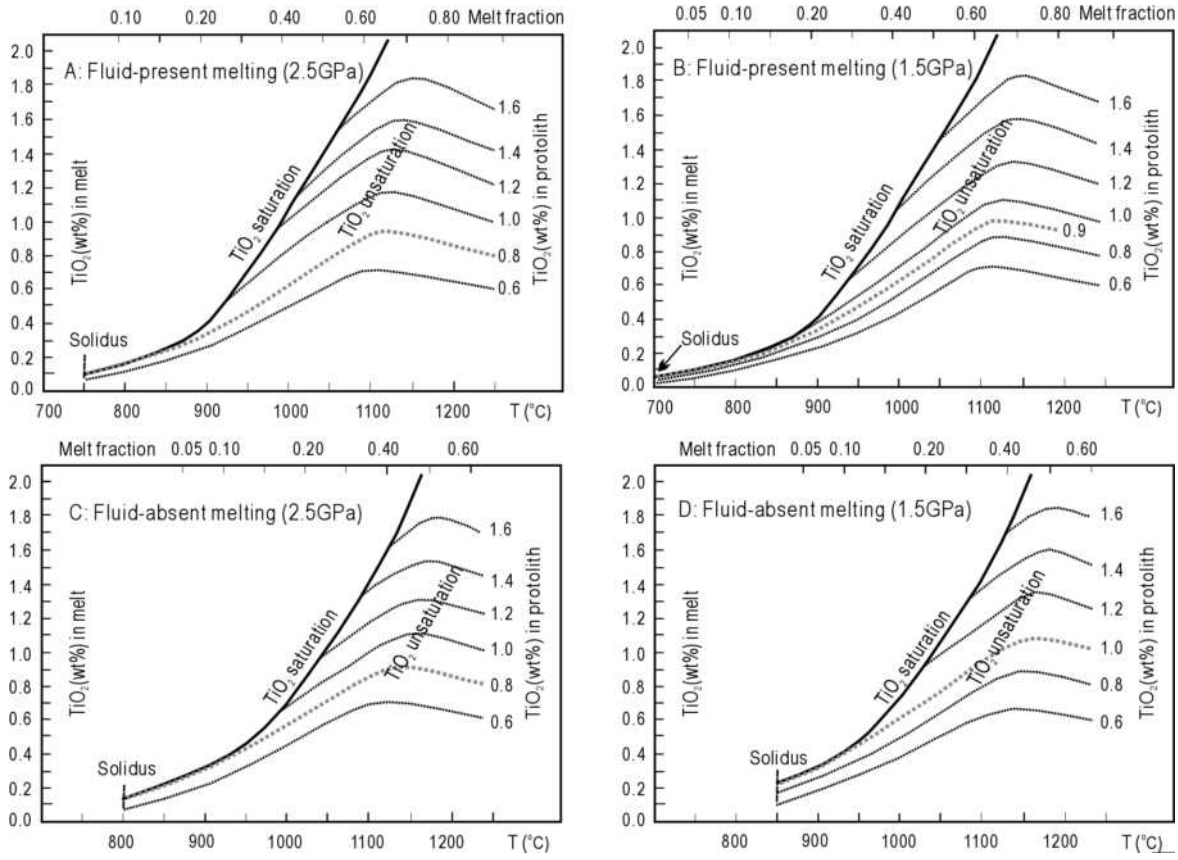

FIGURE 5. Rutile saturation and melt TiO_2 content as a function of temperature or melt fraction (melting degree) at a given protolith TiO_2 content, calculated using the TiO_2 solubility data of melt and minerals and the melt fractions and mineral modes produced during partial melting of hydrous basalts at 1.5–2.5 GPa (see text for details). Four cases are considered: (**a**) fluid-present melting at 2.5 GPa with eclogite as the residue, (**b**) fluid-present melting at 1.5 GPa with amphibole-eclogite (<1050 °C) or eclogite (>1050 °C) as the residue, (**c**) fluid-absent melting at 2.5 GPa with eclogite as the residue, and (**d**) fluid-absent melting at 1.5 GPa with amphibole-eclogite (<1050 °C) or eclogite (>1050 °C) as the residue. The results show that for all cases, only 0.8–1.0 wt% protolith TiO_2 (corresponding to thick dotted curves) is required for rutile saturation during the low-degree (<20 wt%) melting at $T < 900$–950 °C. See text for details and discussion.

high temperatures and pressures, with TiO_2 solubility in H_2O up to 1.9 wt% at 1.0 GPa and 1100 °C, but lower than <0.10 wt% at $T \leq 900$ °C. Recent more precise rutile solubility measurements (Audétat and Keppler 2005; Tropper and Manning 2005; Manning et al. 2008; Antignano and Manning 2008) show that TiO_2 solubility in aqueous fluids is much lower than previously thought. These recent studies demonstrated that TiO_2 solubility in aqueous fluid increases with temperature, pressure, and Na-Al silicate content dissolved in the fluid, with rutile solubility possibly reaching ~0.45 wt% in a high Na/Al fluid (Manning et al. 2008). Metamorphic dehydration of the oceanic crust during subduction is a continuous process. The major fluid release takes place at the transition from wet blueschist or wet amphibolite to nearly dry eclogite facies, where the amount of released fluid is up to 5 wt% in 50–80 km depth (Schmidt and Poli 1998). Such a fluid likely contains silicate components with (Na + K)/Al greater than unity due to incongruent dissolution of albite and micas (Manning et al. 2008). With the maximum TiO_2 solubility of 0.45 wt% in the fluid and 5 wt% aqueous fluid released from a slab, we estimate that only 0.45–4.5% of the TiO_2 budget can be removed by aqueous fluid from the protoliths with TiO_2 ranging from 0.5 to 5.0 wt% (TiO_2 content range of natural basalts), leaving more than 95% of TiO_2 budget in the residue. This indicates that the amount of TiO_2 dissolved in an aqueous fluid released from subsolidus dehydration is insignificant relative to that conserved in the residual solid. Therefore, for a protolith with a given TiO_2 content, the presence of rutile during subsolidus dehydration mainly depends on the TiO_2 solubility in minerals.

In the subsolidus field, breakdown of amphibole and other minor hydrous minerals with increasing pressure to 2.5–3.0 GPa leads to dehydration (Fig. 4), leaving an eclogitic residue (possibly containing lawsonite and/or phengite, depending on temperature). From Figures 2 and 3, we can see that all the possible residual minerals including garnet, clinopyroxene, phengite, and lawsonite dissolve <0.7–0.8 wt% TiO_2 at $T \leq 800$ °C. This indicates that rutile saturation during subsolidus dehydration at the amphibolite to eclogite transition requires only 0.7–0.8 wt% TiO_2 in the protolith. This is consistent with the prevalent presence of rutile in natural eclogites that have experienced metamorphic dehydration (e.g., Zack et al. 2002; Schmidt et al. 2009). Some rutile-bearing veins hosted in eclogites indicate that Ti may have been transported during fluid flow within deep regions of subduction zones (e.g., Gao et al. 2007 and references therein). This seems to be inconsistent with the experimental solubility measurements and the results predicted here. However, the chemical composition of the transporting agent (melt or fluid) causing these veins is uncertain. Moreover, segregation of rutile on a local scale is possible even with small bulk rutile solubility in a fluid, if the fluid repeatedly circulates through the same volume of rock or if fluid flow from a large volume of source rock is focused into narrow channels.

Comparison with previous results at anhydrous conditions

Numerous experiments (e.g., Spandler et al. 2008 and references therein) have been conducted to investigate the phase relations and melting of anhydrous MORB-like eclogite. In several studies (Klemme et al. 2002; Pertermann and Hirschmann 2003; Spandler et al. 2008) attention was paid to rutile stability during the partial melting. The solidus in an anhydrous system is located between 1200 and 1300 °C at 2.0–3.0 GPa, depending on alkali (K_2O and Na_2O) content in the system (Spandler et al. 2008). With starting TiO_2 contents of 1.97 wt% (Pertermann and Hirschmann 2003) and 1.82 wt% (Spandler et al. 2008), minerals close to the solidus at 2.0–3.0 GPa include minor rutile, quartz, and feldspar in addition to clinopyroxene + garnet + felsic melt. Rutile is stable only in the temperature range of 30–50 °C above the solidus, where TiO_2 contents in clinopyroxenes and garnets are mostly at 1.5–2.0 and 0.8–1.0 wt%, respectively, whereas TiO_2 contents in melts range mostly from 3.0 to 6.5 wt% (depending on temperature and melt composition). The experimental results of Klemme et al. (2002) on a dry basaltic composition at 3.0 GPa are similar to those of Pertermann and Hirschmann (2003) and Spandler et al. (2008). Klemme et al. (2002) used their own data on TiO_2 solubility in clinopyroxene and garnet and the melt TiO_2 solubility data of Ryerson and Watson (1987) to calculate the conditions of rutile saturation. They demonstrated that at least ~1.6 wt% protolith TiO_2 content is required for rutile saturation during the partial melting of anhydrous eclogite (see Fig. 2 of Klemme et al. 2002). Partial melting of anhydrous eclogite within a high-temperature environment, such as the mantle plume, will cause rutile to be exhausted rapidly once the melting temperature exceeds the rutile stability. This is consistent with the Ti and HFSE enrichments and the presence of recycled eclogite components in the OIB magmas.

Our results for the hydrous system are very different from those for the anhydrous system. Only 0.7–0.8 wt% TiO_2 is required for rutile saturation during the subsolidus dehydration and 0.8–1.0 wt% TiO_2 is required during the low-degree (<20%) melting at the amphibolite to eclogite transition. With 1.6 wt% TiO_2 in the protolith, rutile is stable up to ~1150 °C and 30–40% melting in the absence of fluid (dehydration melting) and up to ~1050 °C and 50–60% melting in the presence of fluid. The markedly lower protolith TiO_2 required for rutile saturation in the hydrous system relative to the anhydrous system is mainly because of the much lower solidus temperature at hydrous conditions and thus much lower TiO_2 solubility in the melts. The generally lower TiO_2 solubility in clinopyroxene at hydrous conditions (Fig. 2c) may also contribute to the difference. Given that TiO_2 content in the upper kilometer of oceanic crust ranges from 0.7 to 5.0% (Melson et al. 1976) and as it is 1.3–1.6 wt% in the average MORB (Sun and McDonough 1989; Hofmann 1988), our results suggest that nearly all the basaltic protoliths will be saturated with rutile during dehydration or low-degree melting at the amphibolite to eclogite transition. As a persistent residual phase, rutile will result in the characteristic negative Nb-Ta and Ti anomalies in the derived fluids or melts.

Applications to Archean TTG genesis

Archean TTG gneisses represent the oldest felsic continental crust. They record the formation condition of voluminous felsic magmas and the tectonic process that prevailed in the early Earth's history. Experimental and geochemical studies have demonstrated that they are the products of partial melting of hydrous metabasalt (e.g., Martin 1986; Drummond et al. 1996; Rapp and Watson 1995). The tectonic process responsible for the TTG production is a matter of debate. Models proposed

include melting of subducted oceanic crust (Martin 1986; Drummond et al. 1996; and many others) and melting at the base of oceanic plateaus formed above mantle upwelling (Zegers and van Keken 2001; Bédard 2006). The TTG magmas are characterized by strong heavy REE depletion and negative Nb-Ta and Ti anomalies, which require that both garnet and rutile are present in the residue (Barth et al. 2002; Xiong et al. 2005; Bédard 2006; Xiong 2006). Based on the 1.5 GPa of minimum pressure for rutile stability during partial melting of hydrous basalt, the depths for the generation of TTG magmas are constrained to be > ~1.5 GPa (50 km) (Xiong et al. 2005). Recent experiments (Nair and Chacko 2008) demonstrated that garnet abundance during partial melting of hydrous metabasalt increases with increasing pressure. These experiments also showed that melting depths of >48 km are required to have sufficient garnet in the residue for generating the degree of heavy REE depletion in the TTG, consistent with the depths constrained by the pressure of rutile stability (Xiong et al. 2005).

The temperatures for TTG magmas generation are not very clear. Melting experiments of metabasalts (e.g., Sen and Dunn 1994; Rapp and Watson 1995) show that liquids with TTG major element composition can be produced at temperatures <1100 °C by low-degree melting of metabasalt. Indirect inference from the boundaries of amphibole breakdown (releasing H_2O to cause melting) and rutile stability suggests that the *P-T* conditions for TTG generation are at 1.5–2.5 GPa and 800–1050 °C (Xiong 2006). These give only rough temperature ranges for the TTG generation. Above, we have demonstrated that nearly all the basaltic protoliths will be saturated with rutile during low-degree melting at the amphibolite to eclogite transition. This confirms that rutile is a persistent residual phase during TTG generation. As shown in Figure 1, TiO_2 solubility in melts saturated with rutile depends mainly on temperature and melt composition. It is thus possible to constrain the specific temperature of partial melting leading to TTG generation by the solubility data of TiO_2 in melts.

Figure 6 shows that TiO_2 vs. SiO_2 (Fig. 6a) and FM (Fig. 6b) for rutile-saturated melts at 1.5–2.5 GPa and 750–1050 °C compared with those for the Archean TTG. Compositional data of Archean TTG are from the Geochemical Rock Database at http://georoc.mpch-mainz.gwdg.de/georoc/. These felsic rocks have SiO_2 and TiO_2 contents dominantly in the ranges of 66–75 and 0.65–0.10 wt%, respectively. The melts in equilibrium with rutile in our experiments have SiO_2 ranging from 63.0 to 74.0 wt%, generally covering the natural TTG compositions. Figure 6 shows that the TTG rocks in terms of TiO_2 vs. SiO_2 (Fig. 6a) and FM (Fig. 6b) only overlap the experimental and calculated melts with temperatures of 750–1000 °C. More than 95% TTG samples overlap the experimental and calculated melts with temperatures of 750–950 °C, indicating that Archean TTG magmas may have been produced dominantly at 750–950 °C. With the pressure range of 1.5–2.5 GPa for the amphibolite to eclogite transition, the geothermal gradients for the generation of Archean TTG magmas are estimated to be between 10 and 19 °C/km.

The melt generation at 750–950 °C has implications for tectonic models of Archean TTG formation. It indicates that the TTG magmas were produced only at hydrous conditions, because dry partial melting of metabasalt is at much higher

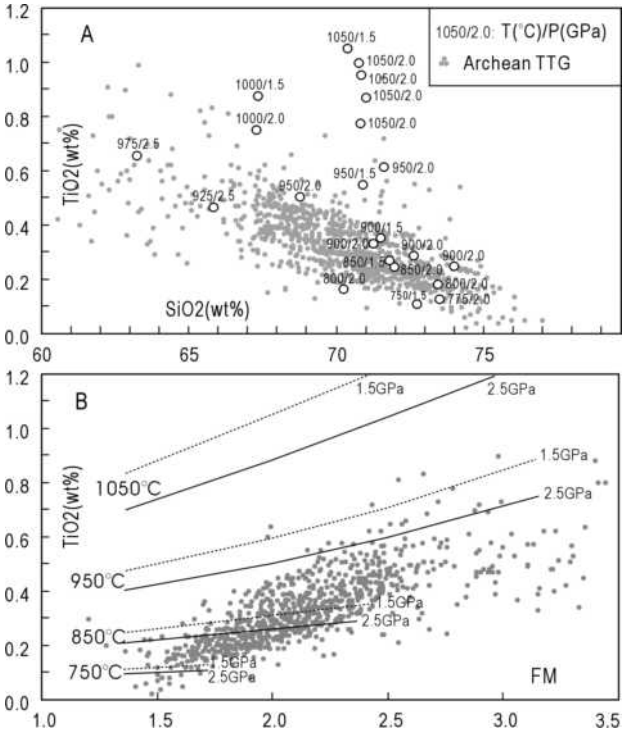

FIGURE 6. TiO_2 vs. SiO_2 (**a**, experimental) and TiO_2 vs. FM (**b**, calculated) in rutile-saturated melts at 1.5–2.5 GPa and 750–1050 °C compared with those of the Archean TTG, showing that the dominant TTG only overlap the experimental and calculated data with temperatures between 750 and 950 °C. Solid lines = calculated temperatures at 2.5 GPa and 10 wt% H_2O; dashed lines = calculated temperatures at 1.5 GPa and 10 wt% H_2O. The Equation 1 was used for the calculations, with the assumption that rutile contains 98 wt% TiO_2 and 2 wt% other components such as FeO, Al_2O_3, and Nb_2O_5, as in natural rutile. The Archean TTG data are from the Geochemical Rock Database in http://georoc.mpch-mainz.gwdg.de/georoc/.

temperatures. A tectonic model should satisfy the requirement that hydrous basaltic rocks be present in the source region of TTG to produce voluminous melts. We argue that models invoking melting at the base of oceanic plateaus are inadequate in explaining the origin of TTG magmas. Plateau root zones are likely dominated by low-Si, high-Mg anhydrous cumulates, which would not be conducive to generating TTG magmas at low temperatures (750–950 °C), because of the absence of water required to depress the melting temperature. Moreover, as argued by Nair and Chacko (2008), oceanic plateaus thicker than 35 km are not known in the geologic record. The root zones of oceanic plateaus are, therefore, not at sufficient depth to stabilize the required amount of garnet for generating heavy REE-depleted TTG. Models involving melting of subducted oceanic crust (Martin 1986; Nair and Chacko 2008) are more consistent with the depth and temperature requirements for generating TTG. The role of subduction processes in the Archean has been disputed on physical grounds that plates did not attain the negative buoyancy to initiate the subduction process (e.g., Davies 1992). Nair and Chacko (2008) presented a modified subduction model to explain the origin of Archean subduction systems and TTG. They hypothesized that intraoceanic subduction systems in the

Archean originated due to gravitational instabilities produced by compositional and density contrasts between converging oceanic plateaus and normal oceanic lithosphere. With a high Archean geothermal gradient, hydrous basalts in subducted oceanic crust would melt to produce voluminous TTG magmas. It is widely accepted that oceanic crust in the Archean was much hotter and more buoyant, leading to subduction at a much lower angle than typical for modern subduction zones. The mantle wedge over an Archean slab was thus very thin and mantle contamination of the TTG magmas, if any, was insignificant (Smithies et al. 2003). This is consistent with the low MgO, Cr, and Ni in the TTG.

Concluding remarks

The TiO_2 solubility in rutile-saturated felsic melts and coexisting minerals was determined at 1.5–3.5 GPa, 750–1250 °C, and 5–30 wt% H_2O. The results, combined with data from the literature, were used to calculate the protolith TiO_2 content required for rutile saturation during partial melting and dehydration of hydrous basalt under conditions relevant to the amphibolite to eclogite transition and to constrain the origin of Archean TTG magmas. The following conclusions are obtained: (1) only 0.7–0.8 wt% TiO_2 in protolith is required for rutile saturation during the subsolidus dehydration and 0.8–1.0 wt% TiO_2 is required for the low-degree (<20%) melting. With 1.6 wt% TiO_2 in the protolith, rutile is stable up to ~1150 °C and 30–40% melting for dehydration melting and up to ~1050 °C and 50–60% melting for fluid-present melting. Thus, nearly all hydrous basaltic protoliths will be saturated with rutile during dehydration or low-degree melting at the amphibolite to eclogite transition, with the derived fluids or melts exhibiting characteristic negative Nb-Ta and Ti anomalies; (2) Archean TTG magmas are characterized by strong negative Nb-Ta and Ti anomalies and are widely accepted to be the products of low-degree melting of metabasalts, with rutile being present in the residue. TiO_2 contents of these magmas may thus have been buffered by the residual rutile during the partial melting. Comparison of natural TTG compositions with experimental melts saturated with rutile in terms of TiO_2 vs. SiO_2 and FM indicates that the dominant TTG magmas were produced at temperatures of 750–950 °C, which requires hydrous conditions. Archean TTG magmas were therefore probably produced by partial melting of hydrous metabasalts in the subducted oceanic crust under high Archean geothermal gradients. With the pressure range of 1.5–2.5 GPa for the amphibolite to eclogite transition, the geothermal gradients responsible are estimated to be between 10 and 19 °C/km.

Acknowledgments

We thank U. Dittmann and H. Schulze for the preparation of polished sections and D. Krausse for help during the electron microprobe analyses, C. McCammon for help during the experiments and N. Huaiwei for help in the calculations. We also thank C. Schmidt and R.L. Linnen for constructive comments that helped to improve the quality of the paper. The work was supported by the Bayerisches Geoinstitut, the NBRP of China (2007CB411303), the NNSF of China (90714011, 40825010), and the CAS project (KZCX2-YW-T004). X.L.X thanks the China Scholarship Council for one-year visit to the BGI. This is contribution no. IS-1077 from GIGCAS.

References cited

Antignano, A. and Manning, C.E. (2008) Rutile solubility in H_2O, H_2O-SiO_2, and H_2O-$NaAlSi_3O_8$ fluids at 0.7–2.0 GPa and 700–1000 °C: Implications for mobility of nominally insoluble elements. Chemical Geology, 255, 283–293.

Audétat, A. and Keppler, H. (2005) Solubility of rutile in subduction zone fluids, as determined by experiments in the hydrothermal diamond anvil cell. Earth and Planetary Science Letters, 232, 393–402.

Ayers, J.C. and Watson, B. (1993) Rutile solubility and mobility in supercritical aqueous fluids. Contributions to Mineralogy and Petrology, 114, 321–330.

Baier, J., Audétat, A., and Keppler, H. (2008) The origin of the negative niobium tantalum anomaly in subduction zone magmas. Earth and Planetary Science Letters, 267, 290–300.

Barth, M.G., Foley, S.F., and Horn, I. (2002) Partial melting in Archean subduction zones: Constraints from experimentally determined trace element partition coefficients between eclogitic minerals and tonalitic melts under upper mantle conditions. Precambrian Research, 113, 323–340.

Beard, J.S. and Lofgren, G.E. (1991) Dehydration melting and water-saturated melting of basaltic and andesitic greenstones and amphibolites at 1, 3, 6.9 kbar. Journal of Petrology, 32, 365–401.

Bédard, J.H. (2006) A catalytic delamination-driven model for coupled genesis of Archaean crust and sub-continental lithospheric mantle. Geochimica et Cosmochimica Acta, 70, 1188–1214.

Brenan, J.M., Shaw, H.F., Ryerson, F.J., and Phinney, D.L. (1995) Mineral-aqueous fluid partitioning of trace elements at 900 °C and 2.0 GPa: constraints on the trace element chemistry of mantle and deep crustal fluids. Geochimica et Cosmochimica Acta, 59, 3331–3350.

Bromiley, G.D. and Redfern, S.A.T. (2008) The role of TiO_2 phases during melting of subduction-modified crust: Implications for deep mantle melting. Earth and Planetary Science Letters, 267, 301–308.

Bureau, H. and Keppler, H. (1999) Complete miscibility between silicate melts and hydrous fluids in the upper mantle: experimental evidence and geochemical implications. Earth and Planetary Science Letters, 165, 187–196.

Davies, G.F. (1992) On the emergence of plate tectonics. Geology, 20, 963–966.

Drummond, M.S., Defant, M.J., and Kepezhinskas, P.K. (1996) Petrogenesis of slab-derived trondhjemite-tonalite-dacite/adakite magmas. Transactions of the Royal Society of Edinburgh, Earth Sciences, 87, 205–215.

Ernst, W.G. and Liu, J. (1998) Experimental phase-equilibrium study of Al- and Ti-contents of calcic amphibole in MORB-A semiquantitative thermobarometer. American Mineralogist, 83, 952–969.

Foley, S.F., Barth, M.G., and Jenner, G.A. (2000) Rutile/melt partition coefficients for trace elements and assessment of the influence of rutile on the trace element characteristics of subduction zone magmas. Geochimica et Cosmochimica Acta, 64, 933–938.

Forneris, J.F. and Holloway, J.R. (2003) Phase equilibria in subducting basaltic crust: Implications for H_2O release from the slab. Earth and Planetary Science Letters, 214, 187–201.

Gaetani, G.A., Asimow, P.D., and Stolper, E.M. (2008) A model for rutile saturation in silicate melts with applications to eclogite partial melting in subduction zones and mantle plumes. Earth and Planetary Science Letters, 272, 720–729.

Gao, J., John, T., Klemd, R., and Xiong, X. (2007) Mobilization of Ti-Nb-Ta during subduction: Evidence from rutile-bearing dehydration segregations and veins hosted in eclogite, Tianshan, NW China. Geochimica et Cosmochimica Acta, 71, 4974–4996.

Green, T.H. (1982) Anatexis of mafic crust and high pressure crystallization of andesite. In R.S. Thorpe, Ed., Andesites, p. 465–487. Wiley, New York.

——— (1995) Significance of Nb/Ta as an indicator of geochemical processes in the crust-mantle system. Chemical Geology, 120, 347–359.

Green, T.H. and Adam, J. (2002) Pressure effect on Ti- or P-rich accessory mineral saturation in evolved granitic melts with differing K_2O/Na_2O ratios. Lithos, 61, 271–282.

——— (2003) Experimentally-determined trace element characteristics of aqueous fluid from partially dehydrated mafic oceanic crust at 3.0 GPa, 650–700 °C. European Journal of Mineralogy, 15, 815–830.

Green, T.H. and Pearson, N.J. (1987) An experimental study of Nb and Ta partitioning between Ti-rich minerals and silicate liquids at high pressure and temperature. Geochimica et Cosmochimica Acta, 51, 55–62.

——— (1986) Ti-rich accessory phase saturation in hydrous mafic compositions at high *P*, *T*. Chemical Geology, 54, 185–201.

Hayden, L.A. and Watson, E.B. (2007) Rutile saturation in hydrous siliceous melts and its bearing on Ti-thermometry of quartz and zircon. Earth and Planetary Science Letters, 258, 561–568.

Hellman, P.L. and Green, T.H. (1979) The role of sphene as an accessory phase in the high-pressure partial melting of hydrous mafic compositions. Earth and Planetary Science Letters, 42, 191–201.

Hofmann, A.W. (1988) Chemical differentiation of the Earth: The relationship between mantle, continental crust, and oceanic crust. Earth and Planetary Science Letters, 90, 297–314.

Huang, W.L. and Wyllie, P.J. (1986) Phase relationships of gabbro-tonalite-granite-water at 15 kbar with applications to differentiation and anatexis. American Mineralogist, 71, 301–316.

Keppler, H. (1996) Constraints from partitioning experiments on the composition of subduction-zone fluids. Nature, 380, 237–659.

Kessel, R., Schmidt, M.W., Ulmer, P., and Pettke, T. (2005) Trace element signature of subduction-zone fluids, melts and supercritical liquids at 120–180 km

depth. Nature, 437, 724–727.
Klemme, S., Blundy, J.D., and Wood, B.J. (2002) Experimental constraints on major and trace element partitioning during partial melting of eclogite. Geochimica et Cosmochimica Acta, 66, 3109–3123.
Klemme, S., Prowatke, S., Hametner, K., and Günther, D. (2005) Partitioning of trace elements between rutile and silicate melts: Implications for subduction zones. Geochimica et Cosmochimica Acta, 69, 2361–2371.
Klimm, K., Blundy, J.D., and Green, T.H. (2008) Trace element partitioning and accessory phase saturation during H_2O-saturated melting of basalt with implications for subduction zone chemical fluxes. Journal of Petrology, 49, 523–553.
Lambert, L.B. and Wyllie, P.J. (1972) Melting of gabbro (quartz eclogite) with excess water to 35 kilobars, with geological applications. The Journal of Geology, 80, 693–708.
Linnen, R.L. (2005) The effects of water on the solubility of accessory minerals in granitic melts. Lithos, 80, 267–280.
Liu, J., Bohlen, S.R., and Ernst, W.G. (1996) Stability of hydrous phases in subducting oceanic crust. Earth and Planetary Science Letters, 143, 161–171.
Lopez, S. and Castro, A. (2001) Determination of the fluid-absent solidus and supersolidus phase relationships of MORB-derived amphibolites in the range 4–14 kbar. American Mineralogist, 86, 1396–1403.
Martin, H. (1986) Effect of steeper Archean geothermal gradient on geochemistry of subduction-zone magmas. Geology, 14, 753–756.
Manning, C.E., Wilke, M., Schmidt, C., and Cauzid, J. (2008) Rutile solubility in albite-H_2O and $Na_2Si_3O_7$-H_2O at high temperatures and pressures by in situ synchrotron radiation micro-XRF. Earth and Planetary Science Letters, 272, 730–737.
Melson, W.G., Vallier, T., Wright, T., Byerly, G., and Nelson, J. (1976) Chemical diversity of abyssal volcanic glass erupted along Pacific, Atlantic, and Indian Ocean spreading centers. In G.H. Sutton, M.H. Manghnani, and R. Moberly, Eds., The Geophysics of the Pacific Ocean Basin and Its Margin, p. 351–361. American Geophysical Union, Washington, D.C.
Mysen, B.B., Virgo, D., and Seifert, F.A. (1982) The structure of silicate melts: Implications for chemical and physical properties of natural magma. Reviews of Geophysics, 20, 353–383.
Nair, R. and Chacko, T. (2008) Role of oceanic plateaus in the initiation of subduction and origin of continental crust. Geology, 36, 583–586.
Patino-Douce, A.E. and Beard, J.S. (1995) Dehydration melting of Bt gness and Qtz amphibolite from 3 to 15 kb. Journal of Petrology, 36, 707–738.
Pertermann, M. and Hirschmann, M.M. (2003) Anhydrous partial melting experiments on MORB-like eclogite: Phase relations, phase compositions and mineral-melt partitioning of major elements at 2–3 GPa. Journal of Petrology, 44, 2173–2201.
Rapp, R.P. and Watson, E.B. (1995) Dehydration melting of metabasalt at 8–32 kbar: Implications for continental growth and crust-mantle recycling. Journal of Petrology, 36, 891–931.
Rudnick, R.L., Barth, M., Horn, I., and McDonough, W.F. (2000) Rutile-bearing refractory eclogites: Missing link between continents and depleted mantle. Science, 287, 278–281.
Rushmer, T. (1991) Partial melting of two amphibolites: Contrasting experimental results under fluid-absent conditions. Contributions to Mineralogy and Petrology, 107, 41–59.
Ryerson, F.J. and Watson, E.B. (1987) Rutile saturation in magmas: Implications for Ti-Nb-Ta depletion in island-arc basalts. Earth and Planetary Science Letters, 86, 225–239.
Schmidt, A., Weyer, S., John, T., and Brey, G.P. (2009) HFSE systematics of rutile-bearing eclogites: New insights into subduction zone processes and implications for the Earth's HFSE budget. Geochimica et Cosmochimica Acta, 73, 455–468.
Schmidt, M.W. and Poli, S. (1998) Experimentally based water budgets for dehydrating slabs and consequences for arc magma generation. Earth and Planetary Science Letters, 163, 361–379.
Schmidt, M.W., Dardon, A., Chazot, G., and Vannucci, R. (2004) The dependence of Nb and Ta rutile-melt partitioning on melt composition and Nb/Ta fractionation during subduction processes. Earth and Planetary Science Letters, 226, 415–432.
Sen, C. and Dunn, T. (1994) Dehydration melting of a basaltic composition amphibolite at 1.5 and 2.0 GPa: Implications for the origin of adakites. Contributions to Mineralogy and Petrology, 117, 394–409.
Smithies, R.H., Champion, D.C., and Cassidy, K.F. (2003) Formation of Earth's early Archean continental crust. Precambrian Research, 127, 89–101.
Spandler, C., Yaxley, G., Green, D.H., and Rosenthal, A. (2008) Phase relations and melting of anhydrous K-bearing eclogite from 1200 to 1600 °C and 3 to 5GPa. Journal of Petrology, 49, 771–795.
Springer, W. and Seck, H.A. (1997) Partial fusion of granulites at 5 to 15 kbar: Implications for the origin of TTG magmas. Contributions to Mineralogy and Petrology, 127, 30–45.
Stalder, R., Foley, S.F., Brey, G.P., and Horn, I. (1998) Mineral-aqueous fluid partitioning of trace elements at 900–1200 °C and 3.0–5.7 GPa: New experimental data for garnet, clinopyroxene, and rutile, and implications for mantle metasomatism. Geochimica et Cosmochimica Acta, 62, 1781–1801.
Sun, S.S. and McDonough, W.E. (1989) Chemical and isotopic systematics of oceanic basalts: implications for mantle composition and processes. In A.D. Saunders and M.J. Norry, Eds., Magmatism in the Ocean Basins, 42, p. 313–345. Geological Society Special Publication, Blackwell Scientific Publications, Boston.
Tropper, P. and Manning, C.E. (2005) Very low solubility of rutile in H_2O at high pressure and temperature, and its implications for Ti mobility in subduction zones. American Mineralogist, 90, 502–505.
Winther, K.T. and Newton, R.C. (1991) Experimental melting of hydrous low-K tholeiite: Evidence on the origin of Archean cratons. Bulletin of the Geological Society of Denmark, 39, 213–228.
Wolf, M.B. and Wyllie, P.J. (1994) Dehydration-melting of amphibolite at 10 kbar: the effects of temperature and time. Contributions to Mineralogy and Petrology, 115, 369–383.
Wood, B.J. and Blundy, J.D. (2001) The effect of cation charge on crystal-melt partitioning of trace elements. Earth and Planetary Science Letters, 188, 59–71.
Xiao, Y., Sun, W., Hoefs, J., Simon, K., Zhang, Z., Li, S., and Hofmann, A.W. (2006) Making continental crust through slab melting: Constraints from niobium–tantalum fractionation in UHP metamorphic rutile. Geochimica et Cosmochimica Acta, 70, 4770–4782.
Xiong, X.L. (2006) Trace element evidence for the growth of early continental crust by melting of rutile-bearing hydrous eclogite. Geology, 34, 945–948.
Xiong, X.L., Adam, J., and Green, T.H. (2005) Rutile stability and rutile/melt HFSE partitioning during partial melting of hydrous basalt: Implications for TTG genesis. Chemical Geology, 218, 339–359.
Zack, T., Kronz, A., Foley, S.F., and Rivers, T. (2002) Trace element abundances in rutiles from eclogites and associated garnet mica schists. Chemical Geology, 184, 97–122.
Zegers, T.E. and van Keken, P.E. (2001) Middle Archean continental formation by crustal delamination. Geology, 29, 1083–1086.
Zhang, R.Y., Zhai, S.M., Fei, Y.W., and Liou, J.G. (2003) Titanium solubility in coexisting garnet and clinopyroxene at very high pressure: The significance of exsolved rutile in garnet. Earth and Planetary Science Letters, 216, 591–601.

MANUSCRIPT RECEIVED NOVEMBER 22, 2008
MANUSCRIPT ACCEPTED APRIL 12, 2009
MANUSCRIPT HANDLED BY MATTHIAS GOTTSCHALK